AGU PUBLICATIONS

Geophysical Research Letters

RESEARCH LETTER
10.1002/2014GL061103

Key Points:
- New aerosol radiative effects above clouds are presented
- Climate models do not reproduce these details well
- Aerosol and cloud properties need to be measured to understand the differences

Correspondence to:
M. de Graaf,
m.degraaf@tudelft.nl

Citation:
de Graaf, M., N. Bellouin, L. G. Tilstra, J. Haywood, and P. Stammes (2014), Aerosol direct radiative effect of smoke over clouds over the southeast Atlantic Ocean from 2006 to 2009, *Geophys. Res. Lett.*, *41*, 7723–7730, doi:10.1002/2014GL061103.

Received 04 JUL 2014
Accepted 17 OCT 2014
Accepted article online 22 OCT 2014
Published online 11 NOV 2014

Aerosol direct radiative effect of smoke over clouds over the southeast Atlantic Ocean from 2006 to 2009

M. de Graaf[1,2], N. Bellouin[3], L. G. Tilstra[2], J. Haywood[4,5], and P. Stammes[2]

[1]Geosciences and Remote Sensing Department, Delft University of Technology, Delft, Netherlands, [2]Satellite Observations Department, Royal Netherlands Meteorological Institute, De Bilt, Netherlands, [3]Department of Meteorology, Reading University, Reading, UK, [4]Met Office, Exeter, UK, [5]Department of Mathematics, CEMPS, University of Exeter, UK

Abstract The aerosol direct radiative effect (DRE) of African smoke was analyzed in cloud scenes over the southeast Atlantic Ocean, using Scanning Imaging Absorption Spectrometer for Atmospheric Chartography (SCIAMACHY) satellite observations and Hadley Centre Global Environmental Model version 2 (HadGEM2) climate model simulations. The observed mean DRE was about 30–35 W m^{-2} in August and September 2006–2009. In some years, short episodes of high-aerosol DRE can be observed, due to high-aerosol loadings, while in other years the loadings are lower but more prolonged. Climate models that use evenly distributed monthly averaged emission fields will not reproduce these high-aerosol loadings. Furthermore, the simulated monthly mean aerosol DRE in HadGEM2 is only about 6 W m^{-2} in August. The difference with SCIAMACHY mean observations can be partly explained by an underestimation of the aerosol absorption Ångström exponent in the ultraviolet. However, the subsequent increase of aerosol DRE simulation by about 20% is not enough to explain the observed discrepancy between simulations and observations.

1. Introduction

Aerosols present one of the major uncertainties in the current understanding of Earth's climate [*Kahn*, 2011]. While models agree that the net direct radiative effect (DRE) of all aerosols combined is negative (i.e., a cooling impact), for some aerosol types, such as biomass burning smoke aerosol, even the sign of the DRE and radiative forcing is in doubt [*Boucher et al.*, 2013; *Sakaeda et al.*, 2011; *Tummon et al.*, 2010]. Nowhere is this uncertainty in direct effect more pronounced than over the southeast Atlantic Ocean [*Myhre et al.*, 2013], where biomass burning smoke aerosols are advected off the African continent above highly reflective, semipermanent stratocumulus clouds. To represent the DRE accurately models represent the geographic distribution and magnitude of the aerosol optical thickness, the aerosol absorption and scattering properties, the geographic distribution of cloud and cloud reflectance, and the vertical profile of aerosols relative to the clouds. Thus, the SE Atlantic is an area that represents a stringent test for current aerosol and climate models.

Many studies have been directed at better characterizing the global aerosol load and the aerosol optical and microphysical properties. Accurate representation of these parameters is essential in climate models in order to characterize the aerosol climate forcing. However, retrieving aerosol properties has proved challenging, due to the heterogeneous distribution of sources of aerosol in both space and time, the large range of aerosol optical and microphysical properties that tend to change with time, and the relatively short lifetime of aerosols, which is typically a few days to a few weeks. A limited number of field campaigns focused on the SE Atlantic (e.g., SAFARI-2000 [*Swap et al.*, 2002]) and have resulted in valuable in situ measurements of aerosol and cloud properties, but for the continuous monitoring of aerosols, daily measurements from satellites are essential [*Kaufman et al.*, 2002]. However, the retrieval of aerosol properties from space is difficult, especially in the presence of clouds. Active remote sensing using lidar can be used to profile the atmosphere above clouds [*Chand et al.*, 2008], and polarization measurements can be used to distinguish the scattering properties of small-sized aerosols and large cloud droplets [*Waquet et al.*, 2009]. Retrieval of aerosol properties in clear sky scenes has improved steadily over recent years [*Kahn*, 2011] but only apply to aerosol properties near cloud edges [*Redemann et al.*, 2009].

A novel method using passive space-based spectrometer measurements from the UV to the shortwave-infrared (SWIR) simultaneously supplies cloud parameters and the aerosol DRE at the top of the atmosphere (TOA) in water cloud scenes with an overlying smoke layer. The cloud parameters are retrieved from the

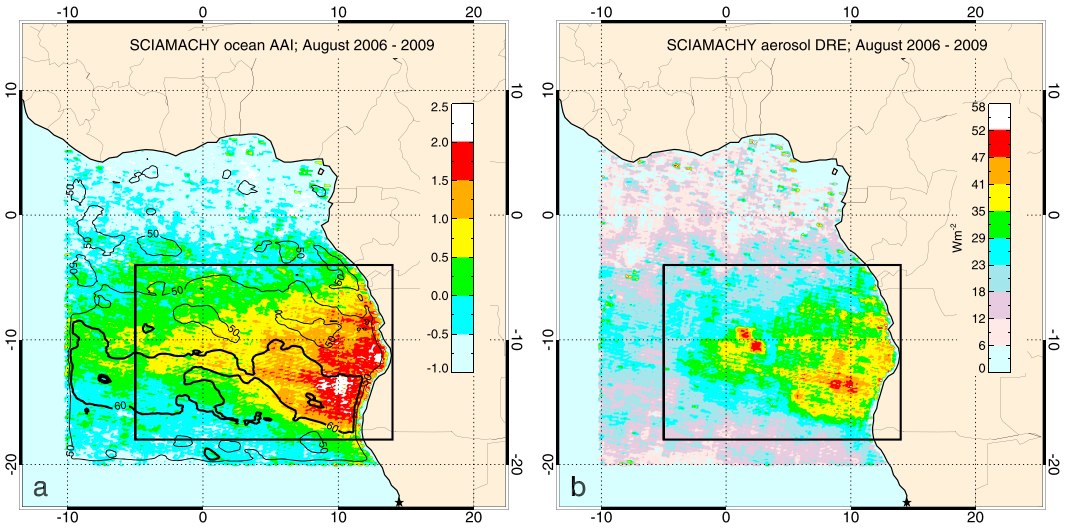

Figure 1. (a) Average SCIAMACHY Absorbing Aerosol Index (AAI) in August 2006–2009 over the southeast Atlantic (filled contour), and SCIAMACHY cloud albedo (contour lines). Shown are the 0.4 and 0.48 cloud albedos, corresponding to 0.5 and 0.6 effective cloud fractions, representing persistent clouds. (b) Average SCIAMACHY aerosol DRE over marine water clouds for August 2006–2009. The rectangle indicates the main outflow region during the biomass burning season.

SWIR reflectances, unbiased by the overlying smoke layer, while the aerosol DRE is retrieved from the reflectances in the entire UV-SWIR range, independently from aerosol parameter assumptions. This differential absorption technique for the retrieval of the aerosol DRE of smoke over clouds is described and quantified in *De Graaf et al.* [2012]. In the current paper the aerosol DRE at the TOA from smoke over clouds during four dry seasons, 2006–2009, is presented and analyzed.

2. Method

The aerosol DRE at the TOA is defined as the change in net (upwelling minus downwelling) irradiance, due to the introduction of aerosols in the atmosphere. Instead of computing the net irradiances with and without the forcing constituent, in our method the DRE at the TOA is determined using the measurement of the upwelling irradiance in the case where aerosols are present, while the irradiance of the case without aerosols is computed using a radiative transfer model. Such an approach has been successfully used over cloud-free ocean regions using aircraft-based radiometers to examine the spectral impacts of mineral dust and volcanic ash [e.g., *Haywood et al.*, 2011; *Newman et al.*, 2012] but never applied to cloudy regions.

The aerosol DRE over clouds at the TOA is estimated using

$$\mathrm{DRE}_{\mathrm{aer}} = \mathrm{SW}^{\uparrow}_{\mathrm{cld}} - \mathrm{SW}^{\uparrow}_{\mathrm{cld+aer}} = \int_{240\ \mathrm{nm}}^{1750\ \mathrm{nm}} \frac{\mu_0 E_0(\lambda)\left(R(\lambda)_{\mathrm{cld}} - R(\lambda)_{\mathrm{cld+aer}}\right)}{B(\lambda,\mu_0)_{\mathrm{cld}}}\mathrm{d}\lambda + \epsilon, \quad (1)$$

where $\mathrm{SW}^{\uparrow}_{\mathrm{cld}}$ is the shortwave upwelling irradiance in the aerosol-free cloud scene, and $\mathrm{SW}^{\uparrow}_{\mathrm{cld+aer}}$ is the shortwave upwelling irradiance in the measured scene; $\mu_0 E_0(\lambda)$ is the solar irradiance incident on a horizontal surface unit at TOA, $R(\lambda)_{\mathrm{cld+aer}}$ is the measured TOA reflectance, $R(\lambda)_{\mathrm{cld}}$ is the simulated aerosol-free cloud reflectance, and $B(\lambda, \mu_0)$ is the anisotropy factor of a scene, which is measure of the angular distribution of the reflected radiation for a scene and used to determine the irradiance from a unidirectional reflectance measurement. The aerosol DRE follows from the integration of the irradiance difference between the simulated aerosol-free cloud scene and measured aerosol polluted cloud scene over the solar spectrum. In our case the integration limits are the range of SCIAMACHY contiguous reflectance measurements (240–1750 nm) [*Bovensmann et al.*, 1999], which is sufficient to capture the entire aerosol effect. A reduction of the upwelling irradiance in the measured scene compared to the simulated aerosol-free scene, the differential absorption, is attributed to the aerosols.

In this study, only pixels with a minimum Fast REtrieval Scheme for Clouds from the Oxygen A band (FRESCO) [*Wang et al.*, 2012] effective cloud fraction of 0.3 are used, to guarantee sufficiently cloudy scenes,

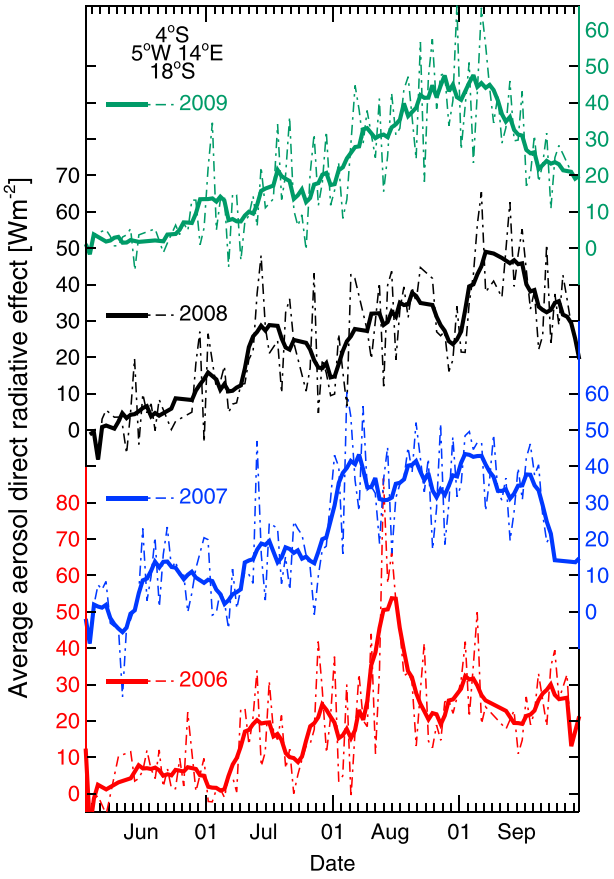

Figure 2. Daily area-averaged aerosol DRE in W m^{-2} for the region 4–18°S, 5°W–14°E (local overpass times from about 9:00 to 10:30 UTC) in 2006–2009 (thin lines) and its 7 day running mean (bold lines).

in which the TOA reflectance is dominated by the clouds. The simulated reflectance spectrum is determined using cloud optical thickness (COT) and the cloud droplet (effective) radius (r_{eff}) inverted from visible and reflectance measurements [*Nakajima and King*, 1990]. Since smoke absorbs strongly in the UV and visible, cloud parameter retrievals using visible wavelengths are biased [*Haywood et al.*, 2004]. However, the absorption optical thickness of small smoke particles is negligible in the SWIR, and unbiased cloud parameters can be determined from the unaffected longwave part of the solar spectrum. Other scene parameters that are used in the retrieval scheme are cloud height, the total ozone column of the atmosphere, and surface albedo. The major advantage of this method is that no assumptions of aerosol optical parameters are needed, thus greatly increasing the accuracy of the retrieved aerosol DRE. The error ϵ in equation (1), due to measurement calibration errors, retrieval uncertainties, and the uncertainty in modeling the aerosol-free scene, was estimated to be about 1% of the incoming irradiance [*De Graaf et al.*, 2012].

The derived aerosol DRE over clouds is compared to model results from the Hadley Centre Global Environmental Model version 2 (HadGEM2) [*Bellouin et al.*, 2011], which includes interactive chemistry and eight species of tropospheric aerosols, including biomass burning aerosol, which is the dominant aerosol type in the region of investigation.

3. Results

The aerosol DRE was computed using SCIAMACHY data over an area from 20°S to 10°N and 10°W to 15°E over the southeast Atlantic Ocean (Figure 1). During the dry season, the African continent is subject to intense and persistent biomass burning, from agricultural practices, deforestation, and domestic wood-burning activities. The smoke from these fires is periodically advected over the Atlantic Ocean under the influence of the dominant anticyclonic circulation over the subcontinent and easterly disturbances [*Garstang et al.*, 1996; *Swap et al.*, 1996]. Figure 1a shows the average Absorbing Aerosol Index (AAI) from SCIAMACHY [*De Graaf and Stammes*, 2005; *Tilstra et al.*, 2012] in August 2006–2009 over the southeast Atlantic Ocean. The AAI is indicative of the presence of UV-absorbing aerosols in both cloud-free and cloudy scenes [*Torres et al.*, 1998] and can be used to show the presence of smoke and desert dust [e.g., *De Graaf et al.*, 2007]. The outflow of smoke over the southeast Atlantic Ocean is concentrated between 0 and 20°S during the June to September period and moves slowly southward as the monsoon progresses [*De Graaf et al.*, 2010]. The smoke usually resides in a layer between 1 and 4 km, overlying a persistent stratocumulus deck, which is present in a layer between about 0.5 and 1 km [*Keil and Haywood*, 2003]. The average SCIAMACHY FRESCO cloud albedo is given in Figure 1a for August 2006–2009, showing the persistence and main location of the stratocumulus clouds.

The SCIAMACHY aerosol DRE over marine clouds was determined for the same region in the months August 2006–2009 using the method described in section 2 (Figure 1b). The aerosol DRE is strongly correlated

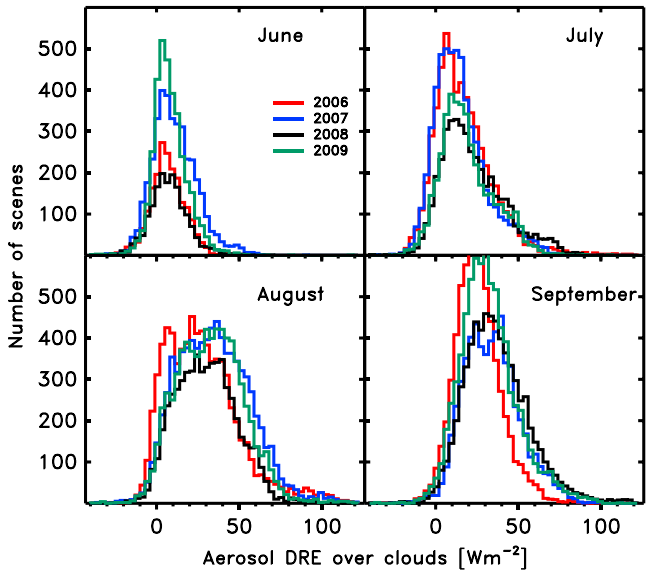

Figure 3. Frequency distributions of aerosol DRE (W m^{-2}) in SCIAMACHY cloud scenes (CF > 0.3) during JJAS in 2006–2009 over the southeast Atlantic region.

with the AAI in this region [*De Graaf et al.*, 2012], because the AAI is an indication of the absorption at UV wavelengths.

The SCIAMACHY aerosol DRE in the southern hemisphere part of the region (indicated by the rectangle in Figure 1) was analyzed for the months June, July, August, and September (JJAS) in the years 2006–2009. Only pixels over the oceans and with an effective cloud fraction larger than 0.3 were processed. In general, aerosol DRE values of about −20 to +150 W m^{-2} were found. The accuracy of the method was estimated at about 8 W m^{-2} per pixel [*De Graaf et al.*, 2012]; the incoming solar irradiance in this season and region is between 900 and 1000 W m^{-2}. The DRE values are higher than found for this region in September 2000 using SAFARI-2000 data to constrain radiative model computations (maximum 65 W m^{-2} [*Myhre et al.*, 2003]). Positive aerosol DRE is a result of absorption in the UV-visible part of the spectrum, attributed to smoke.

The main outflow region is the area between about 4°S to 18°S and 5°W to 14°E, depicted by the rectangles in Figure 1. The area-averaged aerosol DRE over clouds during JJAS 2006–2009 for this region is shown in Figure 2. These are the average aerosol DRE for that area in the morning hours of each day, since SCIAMACHY's overpass time is between about 9:00 and 10:30 A.M. local time. The mean aerosol DRE over clouds for July–August 2006/2007 was 25.9 W m^{-2}, which compares well with the aerosol DRE over clouds averaged over July–October 2006/2007 found with CALIPSO measurements, which had a maximum of about 32 W m^{-2} [*Chand et al.*, 2009]. Figure 2 shows the daily average and the 7 day running mean for each year. The aerosol DRE changes rapidly from day to day, and the patterns are different from year to year, depending on the prevailing synoptic patterns [*Garstang et al.*, 1996]. For example, in August 2006 a thick smoke plume was observed over the southeast Atlantic Ocean, with high values of SCIAMACHY AAI from about 9 to 17 August (not shown). This plume created strong absorption during the second week of August 2006 (cf. Figure 2) and has been used in several observational studies of aerosol absorption over clouds [e.g., *Chand et al.*, 2008; *Waquet et al.*, 2009; *Jethva et al.*, 2013]. The difference between the daily average and the 7 day running mean shows a reduction in the maximum area-averaged aerosol DRE in August 2006 from more than 80 W m^{-2} to about 55 W m^{-2}.

The episodic nature of the aerosol loadings is illustrated further in Figure 3. It shows the frequency distributions of the aerosol DRE over clouds from SCIAMACHY in JJAS 2006–2009, separated per month, for the entire investigated region. Again, only SCIAMACHY ocean pixels with CF > 0.3 are used. The statistics of the various distributions are given in Table 1. Compared to other years, the main biomass burning season of 2006 was very short, concentrated in the month of August. This is illustrated by the large tail of high values in August 2006, creating a higher positive skewness of the distribution. The monthly area average is slightly smaller than in other years, but thick plumes of smoke caused events with very high aerosol DRE. In contrast, in most of June and September 2006 the aerosol DRE was low, with no extreme values in July 2006, creating a symmetric distribution. In 2007 most of the frequency distributions are broader and more symmetric than in 2006, meaning moderate but more continuous absorption by cloud-overlying biomass burning aerosols. In both 2008 and 2009 the onset of the strong absorption period was delayed to the end of August and September, with tails of high-aerosol DRE in September 2008 and 2009. The changing number of events in the various months (the total number of cloud pixels in June 2008 was 1683, and in August 2007 it was 8121) is mainly due to changes in cloud cover in the region and the subsequent satellite pixel sampling.

Table 1. Aerosol DRE Distribution Statistics, Over the Southeast Atlantic Region, as Shown in Figure 3[a]

Month	Year	⟨DRE⟩	σ	γ	n
June	2006	6.75	10.38	0.17	1988
	2007	10.91	13.53	0.60	3897
	2008	7.50	11.82	0.50	1683
	2009	8.17	10.52	0.89	3521
July	2006	16.96	18.09	1.28	5880
	2007	15.08	15.98	0.87	5744
	2008	22.54	19.08	0.76	4335
	2009	18.88	16.15	0.66	4253
August	2006	27.87	22.62	0.99	7515
	2007	34.71	21.84	0.42	8121
	2008	30.06	18.30	0.32	5738
	2009	32.57	19.80	0.33	7414
September	2006	25.68	13.86	0.63	6734
	2007	34.08	16.86	0.43	5980
	2008	36.86	19.29	0.71	6707
	2009	32.14	17.27	0.66	7554

[a]The monthly and area-averaged aerosol DRE above clouds is ⟨DRE⟩ in W m^{-2}, σ is the standard deviation of the distribution (W m^{-2}), γ indicates the skewness, and n is the number of processed SCIAMACHY pixels with cloud fraction larger than 0.3.

The August 2006 event may have been caused by favorable meteorological conditions, episodic emissions, or both. Biomass burning emission data indicate a slightly higher emission rate of black and organic carbon during the first half of August 2006 over southern Africa, but not much. Here the effect of high-aerosol loadings was studied by assuming episodic emission fields in HadGEM2. Normally, emissions are derived in HadGEM2 by linearly interpolating between monthly mean emissions from the updated Global Fire Emission Database biomass burning data sets [*Van der Werf et al.*, 2006], which prevents large changes in emissions when moving from month to month. Figure 4 shows the cloudy-sky shortwave aerosol DRE modeled by HadGEM2 for cloud cover larger than 0.3 in W m^{-2}. The figures show the DRE averaged over the first 8 days (1–8 August 2006), sampled at 9:30 local time. The modeled aerosol DRE over clouds shows a similar spatial pattern as the SCIAMACHY aerosol DRE over clouds, but the modeled values are much smaller than the observed ones. In particular, the model does not show the high values that were found in the observations.

The effect of more episodic emissions of the aerosol plumes is illustrated in Figures 4b and 4c. These show the modeled aerosol DRE over clouds for HadGEM2, when the same total emission as in Figure 4a was used but emitted in shorter bursts. Figure 4b shows the averaged aerosol DRE over clouds from 1 to 8 August when the aerosols were emitted during a 15 day period, and Figure 4c shows the averaged aerosol DRE over clouds when the aerosols were emitted during a 7 day period. The total amount of emitted aerosols is the same in all three model runs. The effect of emissions in bursts is clear: the spatial monthly distribution of the aerosol DRE over clouds remains unchanged, but the maximum values increase when the loadings are larger. However, the monthly averages do not change much. It is 3.80 W m^{-2} for the standard experiment

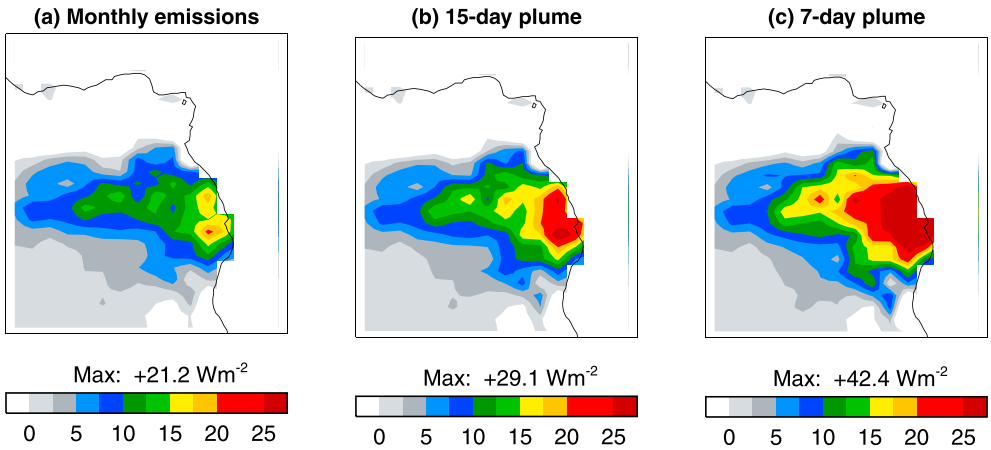

Figure 4. (a) HadGEM2 modeled cloudy-sky shortwave aerosol direct radiative effect in W m^{-2}, averaged over 1–8 August 2006 at 9:30 local time for cloud cover larger than 0.3. The mean aerosol DRE over clouds for this experiment averaged over the whole month is 3.80 W m^{-2}. (b) Same as Figure 4a but with emissions distributed over a 15 day period. Monthly mean is 5.94 W m^{-2}. (c) Same as Figure 4a but with emissions distributed over a 7 day period. Monthly mean is 5.64 W m^{-2}.

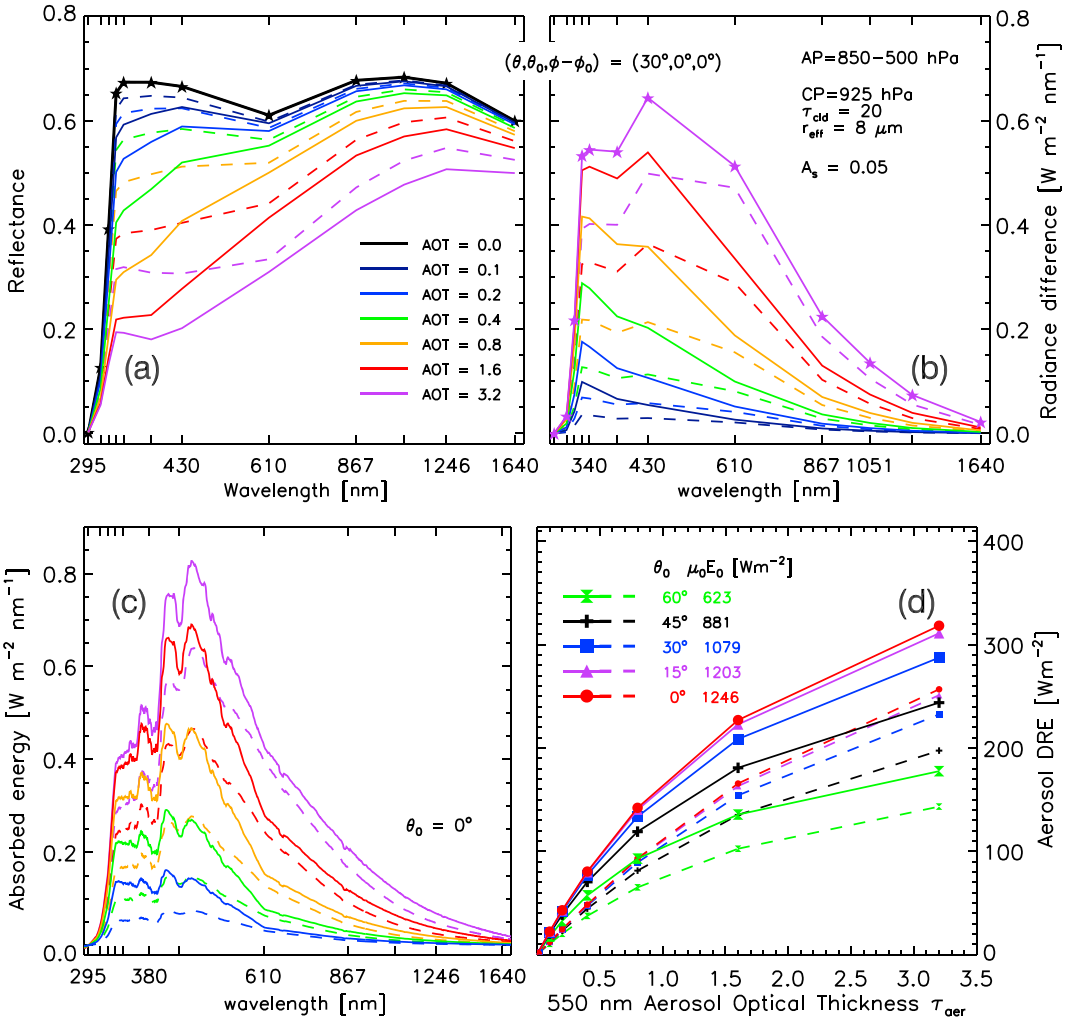

Figure 5. Simulated aerosol DRE for absorbing aerosols over a cloud layer for increasing AOT (shown at 550 nm) with the following simulation setup. Geometry: solar zenith angle $\theta_0 = 0°$, viewing zenith angle $\theta = 30°$ and relative azimuth $\phi - \phi_0 = 0°$; Surface: albedo $A_s = 0.05$; Clouds: pressure (CP) = 925 hPa, droplet size $r_{\text{eff}} = 8$ µm, optical thickness $\tau_{\text{cld}} = 20$; Aerosols: pressure (AP) between 850 and 500 hPa, the solid lines represent the simulations with microphysical parameters fitted to SCIAMACHY measurements, the dashed lines represent the simulations with the microphysical parameters as used in HadGEM2 (aged biomass burning at 60% relative humidity). (a) Simulated reflectance spectra at TOA for the cloud and aerosol layer with increasing AOT; (b) radiance difference between the aerosol-free cloud scene and the aerosol+cloud scenes; (c) absorbed energy for various AOT; (d) Aerosol direct radiative effect of the absorbing aerosols over clouds as a function of AOT at 550 nm at various solar zenith angles.

(Figure 4a), 5.94 W m^{-2} in the case of a 15 day plume, and 5.64 W m^{-2} for the 7 day plume. This is caused by the short residence times of the biomass burning aerosols in the atmosphere, which is about 8 days in HadGEM2, and saturation effects that occur at very high aerosol loadings (see below).

One reason for the discrepancy between the monthly means simulated by the climate model and the monthly mean observations is the underestimation of the absorption of the aerosol model, especially in the UV. The aerosol absorption is highly dependent on the assumed aerosol absorption Ångström exponent and cloud brightness in the model. In Figure 5 the aerosol effect is compared for the aged biomass burning smoke model used in HadGEM2 and the same aerosol size distribution, but a refractive index fitted to the SCIAMACHY measurements. The main change for the fitted model was the much larger absorption Ångström exponent in the UV (2.91 instead of 1.45), in accordance with recent observational studies [*Jethva and Torres*, 2011; *Russell et al.*, 2010; *Bergstrom et al.*, 2007] (see *De Graaf et al.* [2012] for details). The effect is clear from Figure 5a, which shows the simulated reflectance spectrum for absorbing aerosols over a cloud with an optical thickness (τ_{cld}) of 20 and cloud droplet size (r_{eff}) of 8 µm, for

various aerosol optical thickness (AOT). The black line shows the simulated cloud reflectance that would be observed at TOA when no aerosols are present, and the colored lines show the reduced reflectance due to increasing aerosol absorption. Note that the aerosol absorption is strongest at small wavelengths (UV). The dashed colored lines show the aerosol absorption simulated with the microphysical aerosol properties as used in HadGEM2. The aerosol absorption is noticeably underestimated, especially in the UV. This effect is further illustrated in Figures 5b and 5c, where the aerosol effect on the radiance and the absorbed energy is given for both aerosol microphysical models. Finally, in Figure 5d, the total aerosol direct radiative effect over clouds is given as a function of AOT at 550 nm for various solar zenith angles. The total aerosol DRE over clouds is about 20% lower for the HadGEM2 model simulations compared to the SCIAMACHY-fitted aerosol microphysical model. This is insufficient to explain the total discrepancy between the model simulations and the observations. The figure also shows that the change of aerosol DRE with increasing AOT is not linear, but the increase in DRE becomes smaller at higher AOT due to saturation effects at very high aerosol loadings.

4. Conclusions

The aerosol DRE over the southeast Atlantic Ocean during the dry season is poorly understood. The effects of smoke on clouds through absorption of sunlight and the subsequent local heating of the atmosphere, and through their role as cloud condensation nuclei are not represented well in climate models. Accurate measurements of aerosol DRE of smoke over clouds, both from satellite and in situ measurements, can help to understand the radiative interaction between smoke and clouds. The aerosol DRE from June, July, August, and September (JJAS) from 2006 to 2009, as measured by SCIAMACHY over the SE Atlantic shows large differences from year to year. Where 2007 was a year with a long biomass burning season in Africa, with moderate absorption over Atlantic marine clouds throughout the season, in 2006 the absorption peaked very high, during a short high-aerosol loading event in the first part of August.

Currently, climate models are not able to reproduce these details in the measurements [*Myhre et al.*, 2013]. The current study showed that high-aerosol loadings, simulated with short, intense aerosol emissions, increased the maximum aerosol DRE values. The maxima are increased twofold with a fourfold increase of emission rate. Model simulations should therefore include the episodic nature of aerosol emissions in order to correctly estimate these short-term absorption aerosol effects. On the other hand, monthly averaged aerosol DRE are not affected much by different emission distributions, due to the short lifetime of the biomass burning aerosols, and saturation effects of the aerosol DRE in extreme cases.

Simulated monthly averaged aerosol DRE from HadGEM2 are a factor of 5 lower than SCIAMACHY observations. The differences in monthly averaged DRE can on partly be explained by an underestimation of the UV aerosol absorption in HadGEM2. Observations show that smoke from natural fires can have very high absorption Ångström exponents in the UV, due to the presence of organic carbon [*De Graaf et al.*, 2012; *Jethva and Torres*, 2011; *Russell et al.*, 2010; *Bergstrom et al.*, 2007]. The large absorption in the UV is often overlooked by simulations or observational studies that neglect wavelengths shorter than the visible and assume wavelength-independent microphysical properties of smoke. The large absorption in the UV for smoke has been confirmed in many studies and is the basis for the high correlation between the aerosol DRE and AAI [*De Graaf et al.*, 2012]. The current study showed that the aerosol absorption Ångström exponent in the UV currently used for smoke in HadGEM2 reduces the aerosol DRE by 20% as compared to UV-measurement fitted microphysical parameters.

The use of higher aerosol absorption Ångström exponents in climate models will increase the simulated aerosol absorption and DRE, but not enough to explain the discrepancy with the observations. The most likely cause for the remaining discrepancy is the incorrect simulation of the cloud brightness in the model, since aerosol DRE is strongly dependent on cloud fraction and brightness of the scene, but this needs to be confirmed in further studies.

Acknowledgments
This work was funded by the Netherlands Space Office, project AERFORCE (ALW-GO/12-32). SCIAMACHY L1B reflectances used for this study are freely provided by ESA (www.sciamachy.org).

Geoffrey Tyndall thanks two anonymous reviewers for their assistance in evaluating this paper.

References

Bellouin, N., J. Rae, A. Jones, C. Johnson, J. Haywood, and O. Boucher (2011), Aerosol forcing in the climate model intercomparison project (CMIP5) simulations by HadGEM2-ES and the role of ammonium nitrate, *J. Geophys. Res.*, *116*, D20206, doi:10.1029/2011JD016074.

Bergstrom, R. W., P. Pilewskie, P. B. Russell, J. Redemann, T. C. Bond, P. K. Quinn, and B. Sierau (2007), Spectral absorption properties of atmospheric aerosols, *Atmos. Chem. Phys.*, *7*(23), 5937–5943, doi:10.5194/acp-7-5937-2007.

Boucher, O., et al. (2013), Clouds and aerosols, in *Climate Change 2013: The Physical Science Basis. Contribution of Working Group I to the Fifth Assessment Report of the Intergovernmental Panel on Climate Change*, edited by T. F. Stocker et al., Cambridge Univ. Press, Cambridge, U. K., and New York.

Bovensmann, H., J. P. Burrows, M. Buchwitz, J. Frerick, S. Noël, V. V. Rozanov, K. V. Chance, and A. P. H. Goede (1999), SCIAMACHY: Mission objectives and measurement modes, *J. Atmos. Sci.*, *56*(2), 127–150, doi:10.1175/1520-0469.

Chand, D., T. L. Anderson, R. Wood, R. J. Charlson, Y. Hu, Z. Liu, and M. Vaughan (2008), Quantifying above-cloud aerosol using spaceborne lidar for improved understanding of cloud-sky direct climate forcing, *J. Geophys. Res.*, *113*, D13206, doi:10.1029/2007JD009433.

Chand, D., R. Wood, T. L. Anderson, S. K. Satheesh, and R. J. Charlson (2009), Satellite-derived direct radiative effect of aerosols dependent on cloud cover, *Nat. Geosci.*, *2*, 181–184, doi:10.1038/NGEO437.

De Graaf, M., and P. Stammes (2005), SCIAMACHY absorbing aerosol index. Calibration issues and global results from 2002–2004, *Atmos. Chem. Phys.*, *5*, 3367–3389.

De Graaf, M., P. Stammes, and E. A. A. Aben (2007), Analysis of reflectance spectra of UV-absorbing aerosol scenes measured by SCIAMACHY, *J. Geophys. Res.*, *112*, D02206, doi:10.1029/2006JD007249.

De Graaf, M., L. G. Tilstra, I. Aben, and P. Stammes (2010), Satellite observations of the seasonal cycles of absorbing aerosols in Africa related to the monsoon rainfall, 1995–2008, *Atmos. Environ.*, *44*(10), 1274–1283, doi:10.1016/j.atmosenv.2009.12.03.

De Graaf, M., L. G. Tilstra, P. Wang, and P. Stammes (2012), Retrieval of the aerosol direct radiative effect over clouds from spaceborne spectrometry, *J. Geophys. Res.*, *117*, D07207, doi:10.1029/2011JD017160.

Garstang, M., P. D. Tyson, R. Swap, M. Edwards, P. Kållberg, and J. A. Lindesay (1996), Horizontal and vertical transport of air over southern Africa, *J. Geophys. Res.*, *101*(D19), 23,721–23,736.

Haywood, J. M., S. R. Osborne, and S. J. Abel (2004), The effect of overlying absorbing aerosol layers on remote sensing retrievals of cloud effective radius and cloud optical depth, *Q. J. R. Meteorol. Soc.*, *130*, 779–800, doi:10.1256/qj.03.100.

Haywood, J. M., B. T. Johnson, S. R. Osborne, J. Mulcahy, M. E. Brooks, M. A. J. Harrison, S. F. Milton, and H. E. Brindley (2011), Observations and modelling of the solar and terrestrial radiative effects of Saharan dust: A radiative closure case-study over oceans during the GERBILS campaign, *Q. J. R. Meteorol. Soc.*, *137*(658), 1211–1226, doi:10.1002/qj.770.

Jethva, H., and O. Torres (2011), Satellite-based evidence of wavelength-dependent aerosol absorption in biomass burning smoke inferred from Ozone Monitoring Instrument, *Atmos. Chem. Phys.*, *11*, 10,541–10,551, doi:10.5194/acp-11-10541-2011.

Jethva, H., O. Torres, F. Waquet, D. Chand, and Y. Hu (2013), How do A-train sensors intercompare in the retrieval of above-cloud aerosol optical depth? A case study-based assessment, *Geophys. Res. Lett.*, *41*, 186–192, doi:10.1002/2013GL058405.

Kahn, R. A. (2011), Reducing the uncertainties in direct aerosol radiative forcing, *Surv. Geophys.*, *33*(3–4), 701–721, doi:10.1007/s10712-011-9153-z.

Kaufman, Y. J., D. Tanré, and O. Boucher (2002), A satellite view of aerosols in the climate system, *Nature*, *419*, 215–223, doi:10.1038/nature01091.

Keil, A., and J. M. Haywood (2003), Solar radiative forcing by biomass burning aerosol particles during SAFARI 2000: A case study based on measured aerosol and cloud properties, *J. Geophys. Res.*, *108*(D13), 8467, doi:10.1029/2002JD002315.

Myhre, G., T. K. Berntsen, J. M. Haywood, J. K. Sundet, B. N. Holben, M. Johnsrud, and F. Stordal (2003), Modeling the solar radiative impact of aerosols from biomass burning during the Southern African Regional Science Initiative (SAFARI-2000) experiment, *J. Geophys. Res.*, *108*(D13), 8501, doi:10.1029/2002JD002313.

Myhre, G., et al. (2013), Radiative forcing of the direct aerosol effect from AeroCom Phase II simulations, *Atmos. Chem. Phys.*, *13*, 1853–1877, doi:10.5194/acp-13-1853-2013.

Nakajima, T., and M. D. King (1990), Determination of the optical thickness and effective particle radius of clouds from reflected solar radiation measurements. Part I: Theory, *J. Atmos. Sci.*, *47*, 1878–1893.

Newman, S. M., L. Clarisse, D. Hurtmans, F. Marenco, B. Johnson, K. Turnbull, S. Havemann, A. J. Baran, D. O'Sullivan, and J. Haywood (2012), A case study of observations of volcanic ash from the Eyjafjallajökul eruption: 2. Airborne and satellite radiative measurements, *J. Geophys. Res.*, *117*, D00U13, doi:10.1029/2011JD016780.

Redemann, J., Q. Zhang, P. B. Russel, J. M. Livingston, and L. A. Remer (2009), Case studies of aerosol remote sensing in the vicinity of clouds, *J. Geophys. Res.*, *114*, D06209, doi:10.1029/2008JD010774.

Russell, P. B., et al. (2010), Absorption Angstrom exponent in AERONET and related data as an indicator of aerosol composition, *Atmos. Chem. Phys.*, *10*(3), 1155–1169, doi:10.5194/acp-10-1155-2010.

Sakaeda, N., R. Wood, and P. J. Rasch (2011), Direct and semidirect aerosol effects of southern African biomass burning aerosol, *J. Geophys. Res.*, *116*, D12205, doi:10.1029/2010JD015540.

Swap, R., M. Garstang, S. A. Macko, P. D. Tyson, W. Maenhaut, P. Artaxo, P. Kållberg, and R. Talbot (1996), The long-range transport of southern African aerosols to the tropical South Atlantic, *J. Geophys. Res.*, *101*(D19), 23,777–23,791, doi:10.1029/95JD01049.

Swap, R. J., et al. (2002), The Southern African Regional Science Initiative (SAFARI 2000): Overview of the dry season field campaign, *S. Afr. J. Sci.*, *98*(3-4), 125–130.

Tilstra, L. G., M. de Graaf, I. Aben, and P. Stammes (2012), In-flight degradation correction of SCIAMACHY UV reflectances and Absorbing Aerosol Index, *J. Geophys. Res.*, *117*, D06209, doi:10.1029/2011JD016957.

Torres, O., P. K. Bhartia, J. R. Herman, Z. Ahmad, and J. Gleason (1998), Derivation of aerosol properties from satellite measurements of backscattered ultraviolet radiation: Theoretical basis, *J. Geophys. Res.*, *103*(D14), 17,099–17,110, doi:10.1029/98JD00900.

Tummon, F., F. Solmon, C. Liousse, and M. Tadross (2010), Simulation of the direct and semidirect aerosol effects on the southern Africa regional climate during the biomass burning season, *J. Geophys. Res.*, *115*, D19206, doi:10.1029/2009JD013738.

Van der Werf, G. R., J. T. Randerson, L. Giglio, G. J. Collatz, P. S. Kasibhatla, and A. F. Arellano Jr. (2006), Interannual variability in global biomass burning emissions from 1997 to 2004, *Atmos. Chem. Phys.*, *6*(11), 3423–3441, doi:10.5194/acp-6-3423-2006.

Wang, P., O. N. E. Tuinder, L. G. Tilstra, M. de Graaf, and P. Stammes (2012), Interpretation of FRESCO cloud retrievals in case of absorbing aerosol events, *Atmos. Chem. Phys.*, *12*(19), 9057–9077, doi:10.5194/acp-12-9057-2012.

Waquet, F., J. Riedi, L. C. Labonnote, P. Goloub, B. Cairns, J.-L. Deuzé, and D. Tanré (2009), Aerosol remote sensing over clouds using A-train observations, *J. Atmos. Sci.*, *66*, 2468–2480, doi:10.1175/2009JAS3026.1.